The mechanical response of cold bent monolithic glass plates during the bending process

Kyriaki Corinna Datsiou *, Mauro Overend

Glass and Façade Technology Research Group, Department of Engineering, University of Cambridge, Cambridge CB2 1PZ, UK

ABSTRACT

Cold bending of glass involves the straining of relatively thin glass components, (typically plates), at ambient temperatures, and is a low energy and cost effective manner of creating curvilinear forms required in modern glass applications. Cold bending is also popular because it is thought to eliminate the optical imperfections in curved glass plates that arise during alternative and more conventional thermal bending techniques. Experimental and numerical investigations on the cold bending of monolithic glass plates into anticlastic shapes are undertaken and described in this paper. The aim is to characterise the cold bending behaviour during the bending process and to evaluate the surface/optical quality of the curved plates. Two distinct phenomena of interest are observed: (i) a change in the deformation mode that under particular boundary and loading conditions lead to snap-through buckling and; (ii) a local instability termed "cold bending distortion" that appears on curved plates when certain applied displacement limits are exceeded. This cold bending distortion is found to occur at stresses significantly below the fracture strength of the glass plate, but the distortions can be sufficiently large to breach optical serviceability requirements. An optical quality evaluation procedure for predicting the cold bending response and the resulting optical quality of monolithic glass plates are provided at the end of this paper.
© 2016 The Authors. Published by Elsevier Ltd. This is an open access article under the CC BY license (http://creativecommons.org/licenses/by/4.0/).

1. Introduction

The demand for flat glass is high and increasing significantly. Since 2009 float glass production has increased by 5% per annum to meet this demand. The building industry has by far the largest share of this market, and accounts for around 80% of all the flat glass produced [1]. This increase is a direct result of the recent architectural requirements for additional lightness, transparency and natural light in new buildings, leading to an increased demand for larger glass panels. In addition, architectural trends increasingly require the use of glass in curvilinear forms to produce smooth free-form facades [2]. The processes available for producing curved glass can be divided in two categories based on whether heat is involved in the process.

Static mould bending and roller bending are the two most common techniques used to create curved glass and involve heating the glass above the transition temperature (550 °C), so that it becomes viscous. In the static mould bending method (also known as sag bending), the desired curvature of the glass is obtained by allowing the heated flat plate to sag under its self-weight, onto a mould. However, different moulds are required for plates of different curvature therefore, this method is neither energy nor cost efficient. Furthermore, the optical quality of the curved glass plate is very sensitive to imperfections in the mould. An alternative technique that also requires the glass to be heated above its transition temperature is roller bending which can be performed either horizontally or by vertical toughening bending. The former is performed in a horizontal bending toughener during the toughening process of glass; wherein adjustable tilting rollers are used to form the desired shape of the heated glass plate. The glass is then submitted to jets of cold air to create the favourable residual stress profile of toughened glass. On the other hand, in vertical toughening bending, the glass is lowered into the furnace in a vertical position and is pressed onto the mould before being toughened. Roller bending methods therefore have adjustable and re-usable "moulds", but the optical quality of the glass plate is affected by the straightness of the rollers, their position relative to one another and more commonly by roller wave distortion.

The optical quality of glass can be assessed qualitatively with the use of a zebra board plate (consisting of black and white stripes). The waviness of the reflected image on the surface of the glass plate is used to assess whether the level of distortion is acceptable. However, this method is subjective as it relies on the experience of the inspector. More recent quantitative methods

---

include: (i) in-contact with the glass gauges (flat bottom or 3-way-contact gauge) that are conveyed along the direction of the distortion while measuring peak to valley height [3,4]; (ii) non-contact distortion measuring systems involving the use of computer vision and high-resolution cameras [5]. Recommendations such as those set in EN 12150-1:2000 [3] are often used to determine whether the optical quality of the curved plate is acceptable. These limit the amplitude of the roller wave distortion in fully toughened glass to 0.5 mm over a length of 300 mm [5]. It is currently, possible to manufacture toughened glass with significantly smaller roller wave distortion amplitudes. In fact, a limit of 0.25 mm is often prescribed for high-end applications. More information on these thermal bending methods can be found in [6–11].

Cold bending is an alternative, and relatively recent, technique of creating curved glass plates. During this process, the curvature is induced elastically at ambient conditions with a relatively small amount of equipment, thereby, making the process energy efficient and also allowing the bending to be executed on site. Cold bent glass can be used to generate either single or doubly curved forms. Single curvature/developable glass surfaces are easier to form, but they are not as popular in architectural design as doubly curved glass provide a much larger architectural freedom and can be used to create smooth, free form, transparent facades. The glass panels of various curvatures that are required in this kind of applications can be cold bent in shape without any requirement for moulds, therefore, minimising their cost and making cold bending an attractive method of creating curved glass surfaces.

Cold bending involves the application of out-of-plane loads on the glass surface to create the desired shape of the glass plate, the plate is then restrained in its curved state by means of mechanical fixings or structural adhesives. The glass is therefore subjected to permanent bending stresses throughout its service life. Cold lamination bending [12,13] is another recent technique used to restrain the curved glass plate during the cold bending of laminated glass and involves: (i) bending the un-bonded unit of glass plates and interlayer(s) in the desired shape and; (ii) laminating the un-bonded bent unit in an autoclave. In this case, the interlayer preserves the shape of the glass in place though partially, since initial springback is expected when the restraints are removed after the lamination [12,13].

The relatively low strength of annealed glass makes it inappropriate for cold bending applications, as the radius of curvature that can safely be introduced in an annealed glass plate is generally too large to produce significant curvature in the glass plate. Therefore, toughened glass in the form of heat treated (heat strengthened or fully toughened) or chemically toughened glass is often used in such applications. The maximum curvature that can be achieved in cold bent glass has thus far been limited by the maximum surface stresses, generated during the cold bending process (σ_{cb}), that can be safely be resisted by the toughened glass panel throughout its service life:

$$\sigma_{cb} \leqslant \frac{\left(f_{AN,d} - \frac{\sigma_{RES}}{\gamma_{M.RES}} - \sigma_{app} \cdot \gamma_{f,app} \right)}{\gamma_{f,cb}} \tag{1}$$

where $\left(f_{AN,d} - \frac{\sigma_{RES}}{\gamma_{M.RES}} \right)$ is the design strength of toughened glass [14–16], which is the sum total of the design strength of annealed glass,

$f_{AN,d}$, and the design compressive residual surface stresses (negative sign) induced by the thermal/chemical toughening $\left(\frac{\sigma_{RES}}{\gamma_{M.RES}} \right)$; $\sigma_{app} \cdot \gamma_{f,app}$ is the maximum design stress on the surface of the glass induced by loads imposed on the glass during its service life and; $\gamma_{f,cb}$ is an appropriate safety factor to account for variability during the cold bending process.

Recent research [17] has also shown that there is a significant additional contribution to strength in heat treated glass attributable to crack healing, f_{Heal}, therefore, Eq. (1) becomes:

$$\sigma_{cb} \leqslant \frac{\left(f_{AN,d} - \frac{\sigma_{RES}}{\gamma_{M.RES}} - \sigma_{app} \cdot \gamma_{f,app} \right)}{\gamma_{f,cb}} + f_{Heal} \tag{2}$$

There is a growing interest in cold bent glass [18–23] and cold bent glass has already been used in real world applications [24–27]. Two of the most notable examples of completed projects is the 125 m long glass shell of the Strasbourg TGV train station consisting of 6 mm heat-strengthened laminated plates and the glass roof of the Victoria and Albert museum in London that covers an area of 370 m² and consists of cold bent insulated glass units that are point fixed. Yet, to-date no guideline is available for its manufacture/design process.

Cold bending of glass may be an efficient method for creating curved glass surfaces, but the limited research conducted on cold bent monolithic glass plates to-date indicates that it can result in geometric instabilities [28–30]. Staaks and Eekhout [28,29] reported that the free edges of the glass plate change their shape from straight to curved during the cold bending process. Their bending process involved forcing two corners of the plate out-of-plane while the other two were point fixed (Fig. 1a), thereby creating a hyper surface. In particular, two deformation modes were reported. In the first deformation mode, both diagonals were curved and the edges preserved their initial straightness (Fig. 1b). However, when the out-of-plane displacement at the two corners exceeded 16 times the thickness of the plate, a change in the deformation mode was observed [29]; the plate buckled as one diagonal straightens and the edges become curved (Fig. 1c). This phenomenon is noteworthy because curved edges could result in difficulties when fixing the plate to the frame and/or aligning the edges of adjacent glass plates.

A simplified analytical model was also proposed by Eekhout and Staaks [28,29] to predict this buckling instability. The plate was considered as a system of two diagonal strips spanning between the corners of the plate and intersecting at the centre of the plate, and four rods, one along each of the four edges of the plate. By forcing two corners out of plane, bending increases in the diagonals while the rods connecting the corners are stretched creating an additional axial compression in the diagonals. A change in the deformation mode (instability) occurs when the critical Euler buckling stress is exceeded in one diagonal. However, Eekhout and Staaks were unable to obtain good agreement between their simplified analytical model and their numerical results.

This change of curvature has also been described by Galuppi et al. [30] as snap-through buckling. Snap-through buckling, in the case of a plate, is a sudden change of deformation in the direction of the load in the central regions of the plate. Their analytical
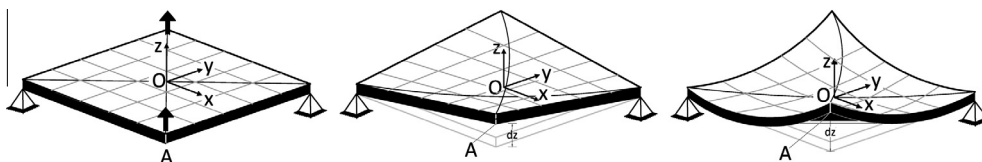

Fig. 1. Deformation modes during the cold bending process (a) undeformed; (b) mode 1 deformation; (c) mode 2 deformation (adapted from [29]).
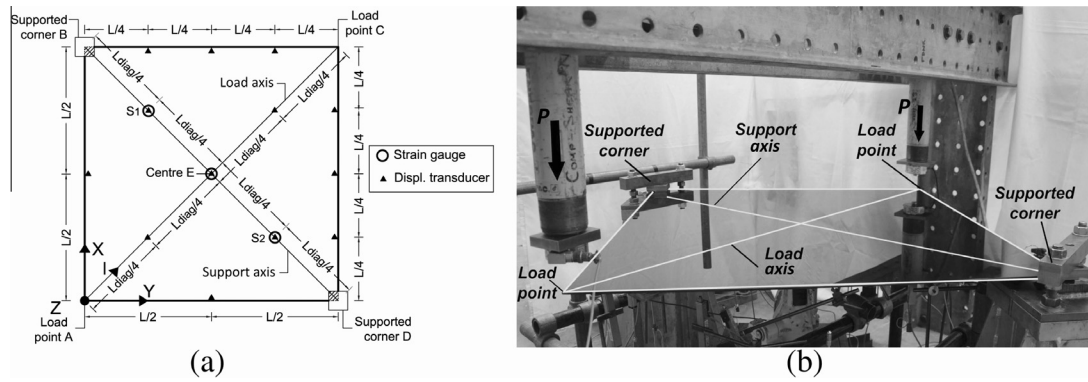
Fig. 2. Cold bending set-up (a) plan view and instrumentation; (b) experimental set-up.

and numerical investigations involved a plate loaded at its four corners; downward loading (negative z, Fig. 2a) was applied at two diagonally opposite corners and upward (positive z, Fig. 2a) at the other two. Their results show that the hyperbolic paraboloid form of the deformed plate changes abruptly and its axes of symmetry are reduced from two to one. This occurs as one of the diagonals straightens while the curvature of the other continues to increase and the edges display significant curvature. An analytical model [30,31], validated by finite element modelling, was proposed by the same authors using a combination of Mansfield's inextensional plate theory and beam theory to account for the double cylindrical shape of the plate. However, the surface quality resulting from the cold bending process is not quantified or investigated, their analytical results have yet to be validated experimentally, and the influence of different boundary conditions have not been investigated.

Apart from energy and cost related benefits, it is thought that cold bending does not affect the optical quality of the glass from its flat state because, unlike thermal bending, viscous flow is not required. However, it was recently reported that optical distortions [32] and unwanted reflections [33] could appear during the bending process thereby bringing into question the optical quality of cold bent glass plates. This geometric instability and the resulting surface quality in monolithic glass plates seem to be overlooked in the limited number of experimental studies on cold bent glass to-date, which have thus far focused on the state of stress of the interlayer in cold bent laminated glass [34,35].

The current study aims to investigate the mechanical response of point-supported, monolithic glass plates that are cold bent into an anticlastic shape, developing the fundamental understanding of monolithic cold bent glass that will eventually also provide the base for future research on the more complicated subject of cold bent laminated glass. The objective is to verify the presence of instabilities during the cold bending process that may lead to permanent optical distortions. Three different cases of boundary conditions (at the supported corners of the plate) are tested

experimentally and modelled numerically. Details of these methods and their results are provided in Sections 2 and 3, respectively. A further interpretation of the results follows in Section 4 that infers the response of the plate during the bending. Furthermore, the validated numerical model is modified in Section 4 to investigate the influence of geometrical characteristics of the plate; orientation of the plate and; load locations during the cold bending process. Finally, an optical quality assessment procedure is proposed in Appendix A to aid designers/manufacturers in achieving cold bent glass with an acceptable optical quality.

2. Method

Numerical modelling and experimental testing were undertaken to investigate the stability of monolithic glass plates during the cold bending process.

2.1. Experimental investigation

Cold bending tests were conducted to produce anticlastic shapes frequently required in free form façades. Anticlastic shapes can be achieved imposing out-of-plane forces along the four edges of the plate. The forces may be placed in a variety of locations e.g. continuously along the edges, at intermediate district locations, etc. The simplest configuration was adopted in this study wherein two corners of the plate (B and D, Fig. 2a) were restrained locally while the remaining two corners (A and C) were subjected to vertical (out-of-plane) loads that were applied incrementally by means of hydraulic jacks (Fig. 2b) actuated by a single manually-operated hydraulic pump. The load was applied at a rate of 1.5–2.5 N/s. However, the geometric response of the monolithic plate is not deemed to be sensitive to the loading rate. Loading was applied up to fracture of the glass plate in order to capture the full extent of the geometric instabilities. The glass plate consisted of $1000 \times 1000 \times 5$ mm thick fully toughened glass and no roller
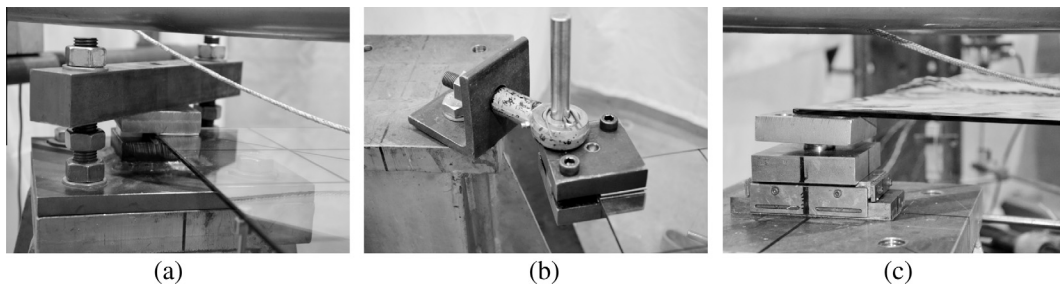

Fig. 3. Boundary conditions: (a) Case CS: clamped supports; (b) Case PS: pin supports; (c) Case RS: roller supports.

Table 1
Translational and rotational restraints at corners B and D for each case of boundary conditions (U = translation; R = rotation).

Case	Description	Restrained DOF	Contact area (mm)	Glass dimensions (mm)	No. of specimens
CS	Clamped supports (fixed in translation and rotation)	$U_x, U_y, U_z, R_x, R_y, R_z$	37.5×37.5	$1000 \times 1000 \times 5$	3
PS	Pin supports (fixed in translation, free in rotation)	U_x, U_y, U_z	37.5×37.5	$1000 \times 1000 \times 5$	3
RS	Roller supports (free in rotation and translation)	U_z	37.5×37.5	$1000 \times 1000 \times 5$	3

wave distortion was detected on the surface of the specimens. The edges were polished prior to toughening in order to reduce the possibility of premature failure from edge flaws.

The following three sets of alternative boundary conditions were used at the locally supported corners B and D (Fig. 3a–c): clamped supports (CS); pin supports (PS) and; roller supports (RS). Table 1 provides an overview of the restrained degrees of freedom for each case. Translational restraints were achieved for Cases CS and PS by clamping the glass between two steel plates with a contact area of 37.5 by 37.5 mm (Fig. 3a). Additionally, in case PS, rotational freedom was provided by an articulated joint in the clamping system (Fig. 3b). Finally, in Case RS, corners B and D were simply supported on spherical supports that were in turn attached to a sliding bearing, thereby allowing rotation and in-plane translation (Fig. 3c); even though the translation in the +Z direction of corners B and D was not restrained mechanically, lifting of the plate from the spherical supports is not an issue in this instance because the reaction forces are not expected to change sign during the testing. Prior to testing, the residual stress profile through the thickness of the fully toughened glass was obtained by means of a scattered light polariscope (SCALP-05, GlassStress Ltd. [36]). Three spot readings were taken on each glass plate, coinciding with the location of the strain gauges that were subsequently attached to the top and bottom surface of the glass plate (Fig. 2a). The mean residual compressive surface stress recorded was σ_{RES} = 85 ± 6 MPa. Three nominally identical glass plates were tested per case of boundary conditions to ensure repeatability of the results. The mean failure load (mean failure corner displacement) recorded at the end of the testing was: (a) 586 ± 37 N/(84 ± 8 mm) for Case CS; (b) 645 ± 11 N/(119 ± 1 mm) for Case PS and; (c) 701 ± 19 N/(135 ± 2 mm) for Case RS.

Displacements and surface stresses were obtained from LVDT displacement transducers and rosette strain gauges, respectively (Fig. 2a). The vertical (out-of-plane) profile of the support axis was acquired by a custom-made surface profilometer that comprised a horizontal wire gauge and a vertical LVDT displacement transducer, to measure the in-plane location, $l_{x,y}$, and out of plane deflection, δ_z, respectively. The surface profilometer was deployed along the support axis at 100 N load intervals.

2.2. Numerical investigation

Numerical models of the experimental set-ups were constructed within Abaqus/CAE 6.12-2, using a static Riks analysis [37] in order to capture any geometric instability that may occur during the cold bending process. The Riks method is an incremental analysis used in non-linear problems. In this method the applied displacements and corresponding deflections are unknowns for each increment and the progress of the solution is evaluated using the arc-length. The initial arc length, Δl_{in}, (set to 0.01), which specifies the percentage of the total displacement that is applied on the first increment of the analysis, and the total arc length, l_{period}, (set to 1.0) provide the initial displacement proportionality factor, $(\Delta \lambda_{in} = \Delta l_{in}/l_{period})$ that determines the first increment of the analysis. Consequently, the procedure consists of a prediction and a corrective phase for each increment. In the prediction phase a suitable starting point is computed for each increment

based on the tangential stiffness derived from the previous converged point on the load–deflection path and the distance along the tangent path that is specified by the arc length; the iterative process of the corrective phase follows afterwards to minimise/eliminate the drift error that is produced by the prediction phase until the solution converges to the equilibrium path. This procedure is automatically implemented in Abaqus with an integrated algorithm. The analysis was set to stop when the displacement at the loaded corners exceeded 100 mm. The self-weight of the plate was modelled as a gravity load, applied prior to the forced displacements at the loaded corners.

The element type and mesh density were selected on the basis of displacement and stress convergence tests in order to provide a good balance between accuracy and computational time. The model consists of twenty-node, quadratic, brick elements with reduced integration properties to prevent shear locking. The glass plate is modelled as 2 elements thick, 80 elements wide and 80 elements long, giving a total of 12,800 elements (Fig. 4). To simulate the boundary conditions that were tested experimentally, the degrees of freedom indicated in Table 1 were restrained accordingly at the 18 solid elements (9 on each layer through the thickness of the plate) within the contact area of the supports. In particular, all of the top and bottom surface nodes of the 18 elements within the 37.5×37.5 mm contact areas of the supports were restrained for Case CS and PS. Contrary, only the bottom surface nodes of the central element (12.5×12.5 mm) of the contact area (37.5×37.5 mm) of the support were restrained for Case RS, simulating the area over the sphere of the spherical support that was restrained from displacing vertically in the experimental set-up. Forced displacements up to 100 mm were applied at the two load points.

Further numerical analyses beyond the experimental set-ups (Table 2a and b) were performed by modifying the validated
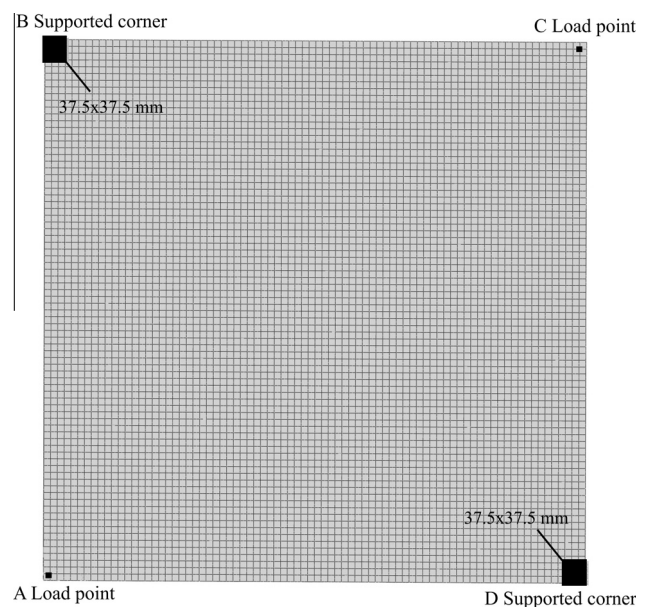
Fig. 4. Numerical set-up.

Table 2
Numerical models: (a) square plates; (b) rectangular plates.

Boundary conditions	Length ratio, LR	Thickness, h (mm)	No. of load points	Orientation of the plate during cold bending	No. of FEA models
(a)					
Case PS	1.00	5*	2	Horizontal	1
Case RS	1.00	5*	2	Horizontal	1
Case CS	1.00	2, 3, 4, 5*, 6, 7, 8	2	Horizontal	7
Case CS	1.00	5	1	Horizontal	1
Case CS	1.00	5	2	Vertical, horizontal-reverse loading	2
Case RS	1.00	5	2	Vertical, horizontal-reverse loading	2
Case CS	1.50	2, 3, 4, 5, 6, 7, 8	2	Horizontal	7
Case CS	2.00	2, 3, 4, 5, 6, 7, 8	2	Horizontal	7
Case CS	2.50	2, 3, 4, 5, 6, 7, 8	2	Horizontal	7
Case CS	3.00	2, 3, 4, 5, 6, 7, 8	2	Horizontal	7

| Boundary conditions	Aspect ratio, AR	Thickness, h (mm)	No. of load points	Orientation of the plate during cold bending	No. of FEA models
(b)					
Case CS	0.50	2, 3, 4, 5, 6, 7, 8	2	Horizontal	7
Case CS	0.75	2, 3, 4, 5, 6, 7, 8	2	Horizontal	7
Case CS	1.25	2, 3, 4, 5, 6, 7, 8	2	Horizontal	7
Case CS	1.50	2, 3, 4, 5, 6, 7, 8	2	Horizontal	7
Case CS	1.75	2, 3, 4, 5, 6, 7, 8	2	Horizontal	7
Case CS	2.00	2, 3, 4, 5, 6, 7, 8	2	Horizontal	7

∗ denotes model corresponding to experimental set-up.

numerical model in order to: (i) quantify the influence of geometrical characteristics, orientation of the plate and load locations on the optical quality of the glass plate and; (ii) propose a brief optical quality evaluation procedure.

3. Experimental and numerical results and observations

The salient results and observations contain the effect of boundary conditions on the load–displacement response and on the final curved shape of the plate; the validation of numerical results; changes in relative stiffness; local changes in curvature; and

surface stress–deflection–load results. These are described in-turn in this section.

The variation of deflection at the centre of the plate (point E, Fig. 2a), $\delta_{E,z}$, versus the load, P, applied on each of the free corners is shown in Fig. 5a. Each case of boundary conditions produced different initial central deflections caused by the self-weight of the glass plate and the influence of the specific boundary conditions. Fig. 5a also reveals that the boundary conditions have a significant effect on the response of the plate during the bending process. When in-plane displacement is unrestrained at the supported corners (Case RS), the load, P, vs. centre deflection, $\delta_{E,z}$, relationship is
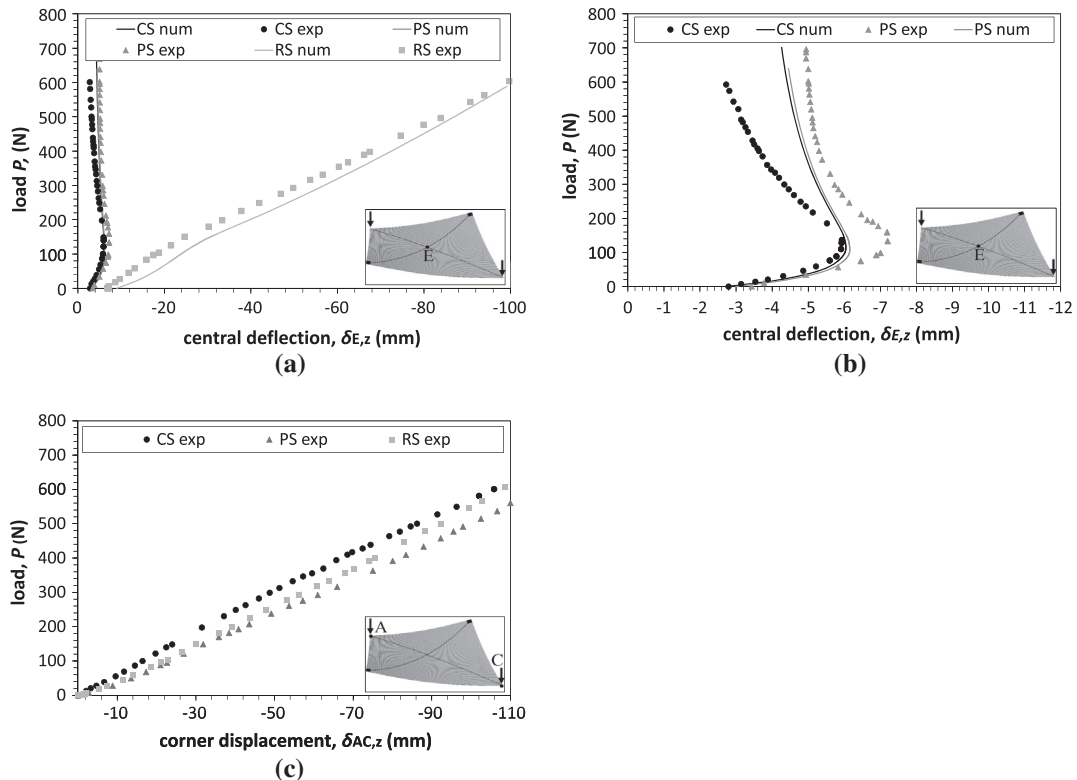
Fig. 5. (a) Load P vs. centre deflection, $\delta_{E,z}$, curves for case CS, PS & RC (exp & num data); (b) close-up of (a) for Case CS & PS and; (c) load P vs. applied displacement, $\delta_{AC,z}$, curves for case CS, PS & RS (numerical data are not shown for clarity).

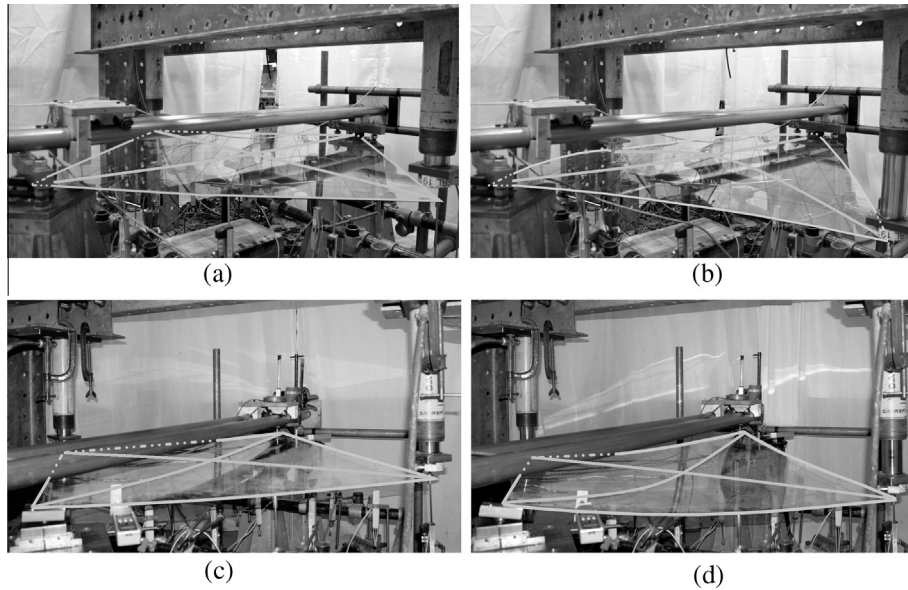**Fig. 6.** Initial and deformed shape: (a) and (b) for case CS and; (c) and (d) for case RS.

almost linear throughout, but when it is restrained the initial linear relationship between load and centre deflection is followed by an end of the proportionality ($P = 110$ N for Case CS and $P = 130$ N for Case PS). When this load is exceeded, the centre of the plate remains approximately stationary until the applied load reaches a value of 150 N for both cases (Fig. 5b). As the load increases further, the deflection of the centre of the plate decreases gradually towards its unloaded position. Furthermore, case CS has a stiffer response compared to the other cases of boundary conditions (Fig. 5c).

It was also observed that the final curved shape of the plate is a function of the boundary conditions (Fig. 6a–d). The surface geometry acquired during the cold bending process is doubly curved. Double curvature, involves bending about two axes and could be either synclastic or anticlastic. In synclastic surfaces (e.g. paraboloid geometry), the principal curvatures are of the same sign i.e. both centres of principal curvatures are located on the same side of the surface. Whereas in anticlastic surfaces (e.g. hyperparaboloid geometry) the centres of principal curvatures are on alternate sides of the surface. The curvature for Case RS was anticlastic throughout the experiment (Fig. 7e and f). This was also observed in the early stages of the bending for the other two cases (Cases CS and PS), however, the anticlastic curvature is disrupted in Cases CS and PS when the applied load, P, at each corner exceeds approximately 250 N (Fig. 7a–d). Some asymmetries are evident in Fig. 7 which can be attributed to minor deviations from symmetry in the initial experimental set-up and are therefore, considered negligible.

The numerical results (Fig. 5a and b) show adequate agreement with the experimental data. Differences appear when the numerical model fails to accurately predict: (a) the post-buckling behaviour of the plate for Case CS, where the numerical model shows a stiffer response and; (b) the load at which the maximum deflection of the centre of the plate occurs for Case PS. These deviations between experimental and numerical results can be attributed to small imperfections in the experimental set-up. Indeed, it was found that minor misalignments in the boundary conditions during iterations of experimental testing resulted in slightly different experimental results but the overall load–displacement responses remained largely unchanged.

A change in the deformation mode was also observed for all three cases of boundary conditions as the curvature of one diagonal increases while the curvature of the other decreases or remains almost unchanged throughout the bending process. In particular for: (a) Case CS and PS: a reduction in the curvature of the support axis occurs after 150 N while the curvature in the load axis continues to increase. The support axis experiences a reduction in absolute values of deflection increments, between subsequent load steps (Fig. 7a and c) whereas the deflection increments of the load axis are almost constant throughout the testing (Fig. 7b and d). This indicates that, the support axis becomes stiffer as the load increases and consequently, substantial deflection is confined to the load axis (Fig. 7b and d); (b) Case RS: an increase in the curvature of the support axis occurs during the bending process while the curvature of the load axis remains almost constant and relatively small (Fig. 7e and f). This suggests that the load axis is stiffer in this case.

Perhaps even more significantly, a change of sign of curvature was observed along the central third of the length of the support axis for Case CS and PS as the load increases beyond 200 N at each corner; the anticlastic curvature is converted to synclastic locally so that the support axis takes the shape of a two-trough ripple (Fig. 7a and c). At this load, the curvature of the central regions of the plate becomes synclastic. This ripple observed in cold bent glass is henceforth referred to as cold bending distortion and can have an undesirable effect on the optical quality of the curved glass similar to roller wave distortion in fully toughened glass. Qualitative images showing the optical distortion on the surface of the glass were captured during the experimental testing. This was achieved by means of a "zebra" board and the use of black spray paint on the bottom surface of the glass to maximise the clarity of the reflected image on the surface of the glass and to create a mirror-like effect. Fig. 8a shows the reflection of the black and white stripes and the edge of the zebra board that reveal the cold bending distortion on the cold bent glass plate. Fig. 8b shows the phenomenon resulting from the numerical model.

Stress and deflection data are used in the following 4 load ranges to describe the mechanical response with increasing load of a cold bent glass plate for Case CS. Principal strain data obtained from strain gauges showed that the directions of the principal strains are aligned to the support and the load axes. In particular, the angle between the support axis and the direction of the maximum principal stresses, θ, is relatively small and ranges between $-4.3°$ and $1.6°$ during the testing for all the top and bottom stresses of points E and S_1 (Fig. 2a), making the in-plane shear strain
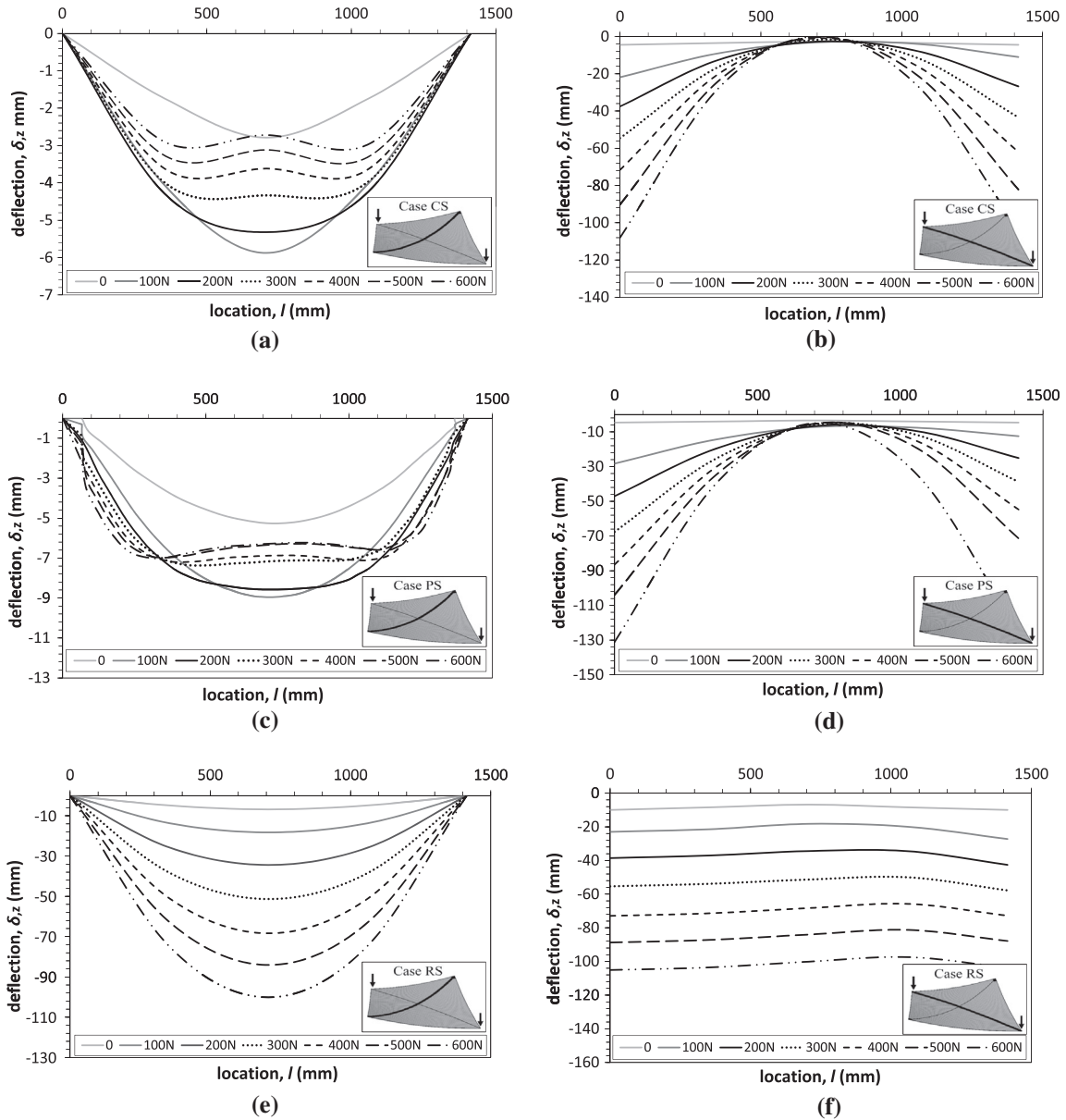
Fig. 7. Experimental results showing the support and load axis profile at 100 N load increments for: (a) and (b) case CS; (c) and (d) case PS and; (e) and (f) case RS.

between the two axes negligible. Therefore, the strain and stress data that are used below refer to the direct principal values in the direction of the support axis.

(1) *0–110 N:* During the initial stages of the bending process, the central regions of the plate displace away from the initial flat position creating an anticlastic shape, until the applied load reaches 110 N (Fig. 5b). Strain gauge data and corresponding stresses, at the top surface of the plate along the direction of the support axis BD (Fig. 2a), σ_{sd}, show that up to this load, in-plane compressive stresses are present along its length (Fig. 9a).

(2) *110–150 N:* When the load exceeds 110 N the central regions of the plate cease to deflect vertically and remain relatively stationary up to a load of 150 N (Fig. 5b). This is accompanied by a corresponding reduction in the top surface compressive stresses at the centre of the plate (Fig. 9b and c), whereas the top surface compression in the outer third regions (point S_1 and S_2, Fig. 2a) of the support axis (Fig. 9d) continues to increase.

(3) *150–250 N:* As the load increases beyond 150 N, a change in the deformation mode occurs; the load axis continues to acquire more curvature, while the curvature of the support axis diminishes (Fig. 7a and b). Within this load range, the centre of the plate starts to deflect back towards its unloaded position (Fig. 5b). This coincides with the accumulation of top surface tensile stresses in the central regions of the plate, $\sigma_{sd,E}$, (Fig. 9a–c). However, even after this change in the deformation mode, top surface compressive stresses still dominate the outer third parts of the support axis (points S_1 and S_2 from Fig. 2a) (Fig. 9a and d). The maximum value of compression (7 MPa) at S_1 and S_2 is reached at the load of 250 N (Fig. 9d).

(4) *above 250 N:* At 250 N, the top surface compressive stresses along the support axis start to decrease, as seen at points S_1 and S_2 (Fig. 9d). At this load a gradual change of the double curvature of the plate from synclastic to anticlastic occurs in the central regions of the plate. This leads to the appearance of the cold bending distortion that manifests itself as a sinusoidal deformation along the support axis BD (Fig. 7a and b).
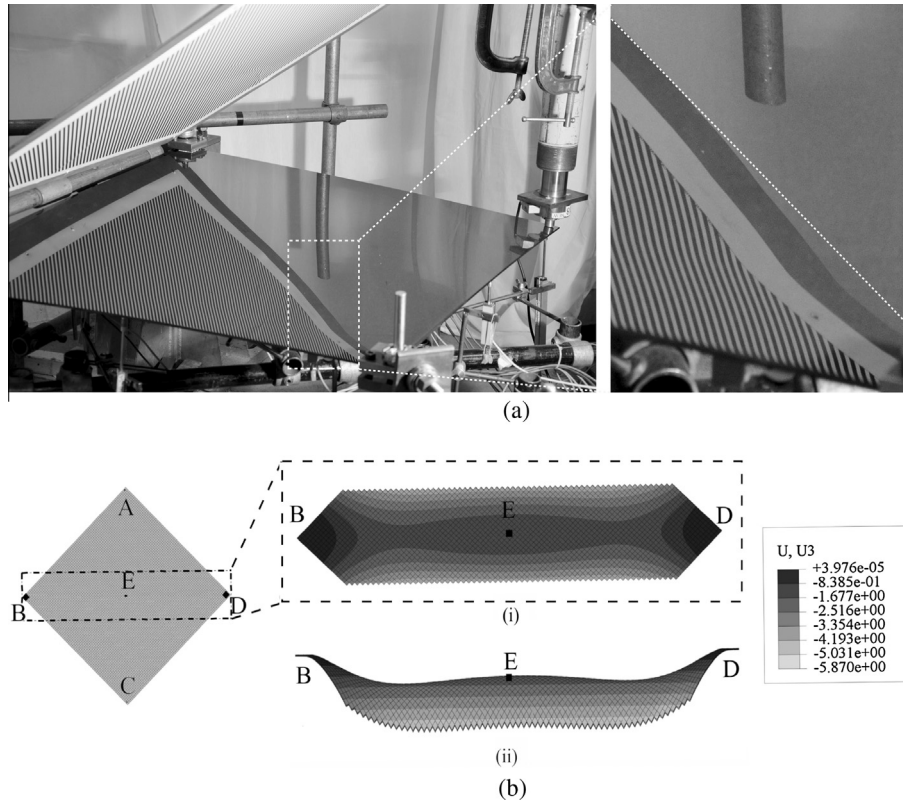
Fig. 8. Cold bending distortion: (a) distorted reflection of zebra board on cold bent glass and; (b) cold bending distortion in the numerical model: (i) top view and; (ii) side view (exaggerated 40 times vertically).
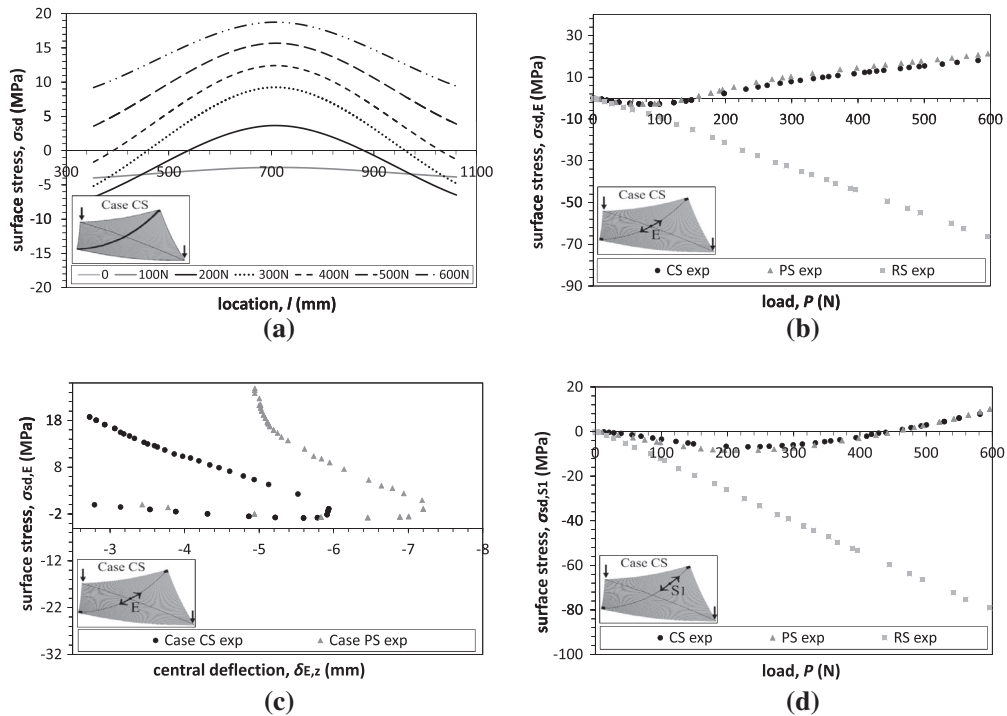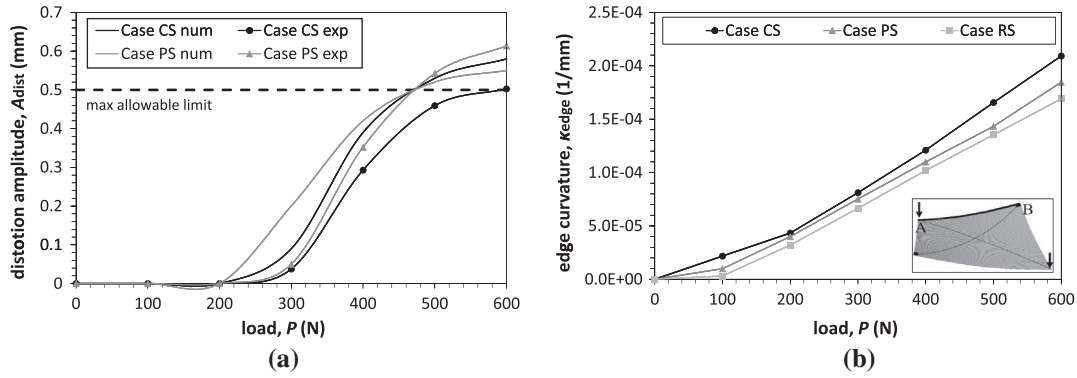

Fig. 9. Experimental surface stress results in the direction of the support axis for: (a) the support axis (case CS) in loading steps of 100 N, σ_{sd}; (b) the centre of the plate, $\sigma_{sd,E}$, vs. the applied load; (c) the centre of the plate, $\sigma_{sd,E}$, vs. the centre deflection and; (d) point S_1 (Fig. 2a), $\sigma_{sd,S1}$, vs. the applied load.

Fig. 10. (a) Cold bending distortion amplitude with increasing load for Case CS & PS (experimental and numerical data) and; (b) experimental curvature results of the edges of the glass plate.

The amplitude of the cold bending distortion, A_{dist}, i.e. the height difference between its highest and lowest point (peak to trough), continues to increase with increasing load until the end of the test at 600 N (Fig. 10a). The same applies to the curvature of the edges, κ_{edge}, of the plate (BA, BC, DA and DC, Fig. 2a).

A response similar to that described above was observed for Case PS. However, for Case RS, neither cold bending distortion nor the corresponding tensile stresses on the top surface of the support axis were observed. The top surface stresses in the central regions of the RS plate therefore remained in compression throughout the cold bending process (Fig. 9b).

4. Discussion

4.1. Interpretation of the mechanical response of the plate

Two phenomena of interest were observed during the cold bending process: (a) a change in the deformation mode and; (b) the cold bending distortion. The cold bending distortion was only apparent in Cases CS and PS. The response for Case CS can be interpreted as follows:

The development of surface tensile strains in the central regions of the plate (150–250 N, Fig. 9b) leads to an increase in the flexural stiffness of the central parts of the support axis. Therefore, significant deflections are confined to the load axis AC while the support axis starts to decrease in curvature (change in the deformation mode, Fig. 7a and b).

Strain profiles at points S_1 and E (Fig. 11a and b), reveal that membrane effects are significant along the support axis while the load axis is predominantly subjected to bending effects. The axial force that is developed at points S_1 and E during the testing can be determined from the membrane strains at these points (Fig. 12). The results show that the axial compression initially increases for both points S_1 and E until a load of 100 N. Above this load the axial force decreases at point E and is finally transformed to axial tension (180 N) while the axial compression continues to increase at S_1. Eventually, the axial compressive stress at point S_1 reaches a critical value of 25 N/mm at a load of 250 N (Fig. 12), and eventually leads to a local instability (local buckling) and the
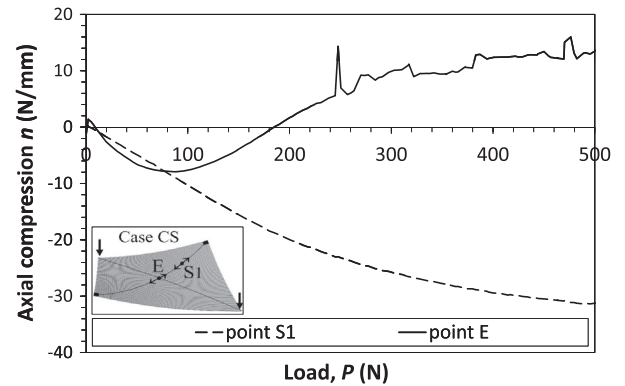
Fig. 12. Axial force along the support axis for points S_1 and E during the testing.
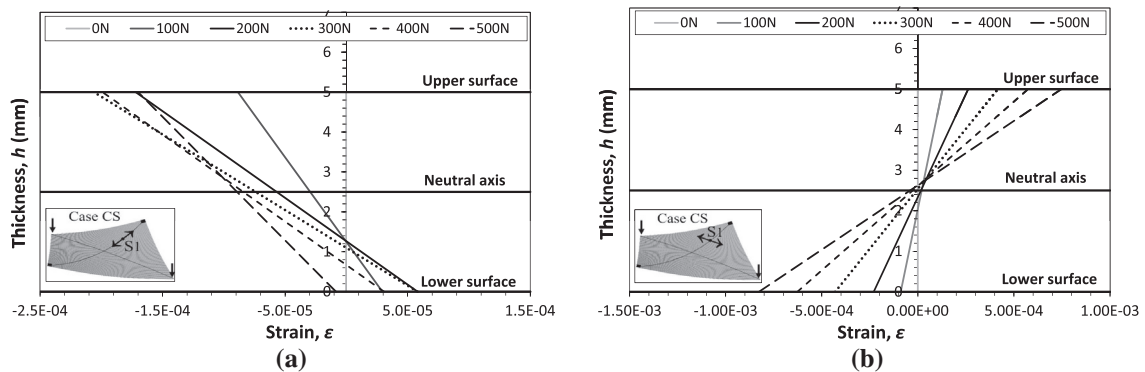
Fig. 11. Cross-sectional strain for point S_1 along: (a) the direction of the support axis and; (b) along the direction of the load axis.

Table 3
Numerical and experimental data for the stress and the amplitude of the cold bending distortion during the bending process.

Case CS					Case PS				
P (N)	$\delta_{AC,z,num/exp}$ (mm)	$A_{dist,num}$ (mm)	$\sigma_{t,num,max}$ (MPa)	$A_{dist,exp}$ (mm)	P (N)	$\delta_{AC,z,num/exp}$ (mm)	$A_{dist,num}$ (mm)	$\sigma_{t,num,max}$ (MPa)	$A_{dist,exp}$ (mm)
0	0	0.00	0.0	0.00	0	0	0.00	0.0	0.00
100	−18	0.00	35.9	0.00	100	−18	0.00	40.7	0.00
200	−32	0.00	54.9	0.00	200	−40	0.00	55.6	0.00
300	−47	0.19	70.0	0.04	300	−55	0.20	68.2	0.05
400	−61	0.39	83.4	0.29	400	−69	0.42	79.7	0.35
500	−76	0.54	95.8	0.46	500	−84	0.52	95.6	0.54
600	−90	0.64	107.5	0.50	600	−105	0.55	105.7	0.61

corresponding gradual change of the double curvature from anticlastic to synclastic in the central regions of the plate (cold bending distortion, Fig. 7a). The sharp peak of axial tension that is developed at point E (Fig. 12) at the load of 250 N is a manifestation of this instability.

The difference in Case RS is that the supported corners of the plate (B and D) are free to displace in-plane. The absence of in-plane reaction forces allows the support axis to acquire significantly smaller radii of curvature than those of the previous cases (CS and PS) (Fig. 7a, c, and e). As the load increases, the curvature of the support axis increases while the load axis retains a constant curvature (change in the deformation mode). The cold bending distortion is not triggered in Case RS when the load is applied in the same direction as the self-weight. However, as shown in Section 4.2.2, the cold bending distortion in Case RS is sensitive to the direction of the load with respect to initial imperfections. Therefore, the cold bending distortion can be attributed to the forcing of the plate into a non-developable surface generated by the plate geometry, the boundary conditions and out-of-plane loads.

The numerical and experimental results showing the progress of the cold bending distortion during the bending process for Case CS and PS are summarised in Table 3. The cold bending distortion initially occurs when the applied load P exceeds 200 N at each of the two free corners. At this load, the maximum tensile stress, $\sigma_{t,max}$, on the surface of the glass plate, is 54.9 MPa and 55.6 MPa for Case CS and PS, respectively. This is significantly lower than the design strength of fully toughened glass which can be approximately estimated using part of Eq. (1) as follows:

$$f_{AN,d} - \frac{\sigma_{RES}}{\gamma_{M,RES}} = 30 - \frac{-85}{1.20} = 100.8 \text{ MPa}$$

where σ_{RES} is derived from the SCALP measurements.

Therefore, in both cases the cold bending distortion precedes the fracture of the glass plate and potentially exceeds a serviceability limit due to the optical distortions occurring in the curved plate. The amplitude of the cold bending distortion, A_{dist}, can indicate whether distortions are visually acceptable or not. European standard limits the amplitude of roller wave distortion in fully toughened glass to no more than 0.5 mm [3]. This limit is exceeded during the cold bending process at an applied load of: P = 420 N (experimental and numerical data) for Case PS and; P = 480 N (numerical data) and P = 600 N (experimental data) for Case CS (Fig. 10a).

Overall, the experimental and numerical results support Galuppi's [30,31] and Staaks's [28,29] observation that one diagonal straightens during the bending while the other becomes more curved (Fig. 7a–f). However, this change in the deformation mode occurred gradually with increasing load and no general limit point buckling (snap-through instability), such as that suggested by Galuppi [30] was observed in these cases (Fig. 5b).

It is however, shown (see Section 4.2) that snap-through buckling could be triggered under a specific case of boundary and loading conditions. Additionally, the increase in the curvature of the edges, κ_{edge}, (BA, BC, DA and DC, Fig. 2a) also occurred gradually without any sudden change in shape (Fig. 10b).

4.2. Parametric analysis

The onset of the cold bending distortion is expected to be a function of the geometrical characteristics, the orientation of the plate and the load locations during the bending process. These parameters were investigated by modifying the numerical model to suit (Table 2) and the results are discussed in-turn.

4.2.1. Geometrical characteristics of the plate

Further numerical simulations were performed to investigate the influence of the initial geometry of the glass plate (thickness, edge length and aspect ratio) on the development of the cold bending distortion. Forced displacements up to 200 mm were applied at the two free corners of the plate for Case CS.

The results show that the cold bending distortion occurs at a smaller values of applied displacement during the cold bending process for thinner plates (Fig. 13a). However, cold bending of thicker glass plates leads to larger values of maximum distortion amplitude. The recommended limit for roller wave distortion (0.5 mm) is exceeded when the thickness of the glass plate $\geqslant$ 4 mm. This may compromise the optical quality of the cold bent plate.

Square plates with different edge length and a thickness of 5 mm were also investigated. This was done by varying the length ratio, which is the ratio of the edge length of the tested plate, L_p, over the edge length of the reference plate, $L_{p,0}$ = 1000 mm, $LR = L_p/L_{p,0} = L_p/1000$. Numerical results showed that the cold bending of plates with larger length ratio, LR, produces smaller values of amplitude of cold bending distortion for the same applied displacement at the free corners (Fig. 13b). The maximum distortion amplitude for plates with an edge length $\geqslant$ 2000 mm and a thickness of 5 mm does not exceed the limit of roller wave distortion (0.5 mm) up to an applied corner displacement of 200 mm.

The change in the deformation mode was also found to be a function of the aspect ratio, AR, of the plate (Fig. 14a). It was found that square plates required the smallest magnitude of forced displacement at the free corners, δ_{dist}, to trigger cold bending distortion (Fig. 14b), and exhibited the smallest distortion amplitude among the aspect ratios investigated (0.5 $\leqslant$ AR $\leqslant$ 2.00).
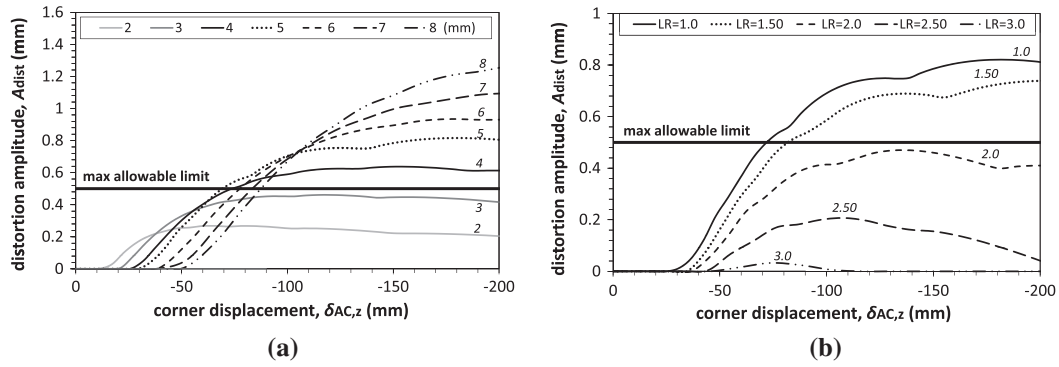
Fig. 13. Amplitude of the cold bending distortion for plates of different: (a) thickness and dimensions of 1000 × 1000 mm and; (b) length ratio, LR, and thickness of 5 mm (numerical data).
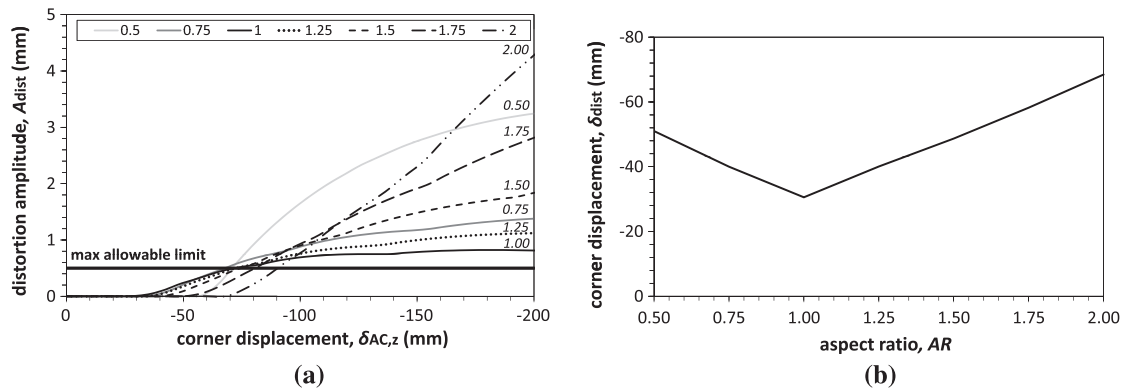
Fig. 14. Influence of aspect ratio for 5 mm thick plates: (a) amplitude of the cold bending distortion and (b) applied displacement at the onset of the cold bending distortion (numerical data).

4.2.2. Cold bending orientation and load locations

Possible influences of plate orientation with respect to gravity and load locations were also investigated numerically. In particular, the orientation of the plate was considered pertinent as it changes the influence of the self-weight on the cold bending distortion. The plate was modelled for Case CS and RS: (a) horizontally (*Hor*), with the corner displacement applied in the same direction as the self-weight (this is identical to the experimental and numerical models described in this paper in Sections 2 and 3); (b) horizontally (*Hor-reverse*), with the corner displacement applied in the opposite direction to the self-weight and; (c) vertically (*Ver*), so that the self-weight acts in the plane of the glass plate and its influence can be considered negligible.

The results show that initial deflections in the plate's flatness caused by the self-weight have an important influence in the mechanical response of the plate. In *Hor* and *Ver* testing, no snap-through buckling occurs (Fig. 7a,b and e,f and 15a,b and c, d). However, in *Hor reverse* testing the plate exhibits a change of sign of curvature in both the load and the support axis (Fig. 15e,f and g,h). This is observed at a load of 63 N and a corner displacement of 10 mm for Case CS, while for Case RS the load and corner displacement are 78 N and 15 mm, respectively. Fig. 16a and b shows the deformed plate shape before and after the snap-through instability for Case RS. Therefore, snap-though instability is triggered when the out-of-plane loads are applied in a direction opposite to the initial out-of-plane deflection induced by self-weight (or other surface imperfections) of the plate. Overall, one of two possible configurations occur during the initial stages of

the cold bending process, shown in Figs. 7e and f/15e and f for Case RS and Figs. 7a and b/15g and h for Case CS. The resulting configuration is based on the direction of the external cold bending loads with respect to gravity; when the self-weight acts in the same direction as the external loads, the configuration that is initially formed as a result of the self-weight alone, is maintained when the external loads are applied and global instabilities are prevented (Fig. 7a,b and e,f); however, snap-through instability occurs when the self-weight and the external loads act in opposite directions as the plate changes suddenly from one configuration to the other (Fig. 15e,f and g,h). In both cases where snap-through instability is noticed, increasing the applied corner displacement further, eventually leads to cold bending distortion (Fig. 16c) (CS and RS).

Table 4 summarises both phenomena (snap-through instability and cold bending distortion) for the different plate orientations of Case CS and RS. It is clear that cold bending distortion always follows snap through buckling, but that snap-through buckling is not always a precursor of cold bending distortion. Finally, Fig. 17 shows that snap-through buckling has a negligible effect on the amplitude of the cold bending distortion.

The influence of the number of the load points, *LP*, was also investigated numerically for Case CS. An increase in the plate's stiffness is observed when the number of load points, *LP*, is decreased to 1 and the number of supported corners is simultaneously increased to 3. The onset of the cold bending distortion occurs at larger applied displacement values during the bending process (50 mm of applied displacement in comparison to 30 mm) while the value of the distortion amplitude is significantly
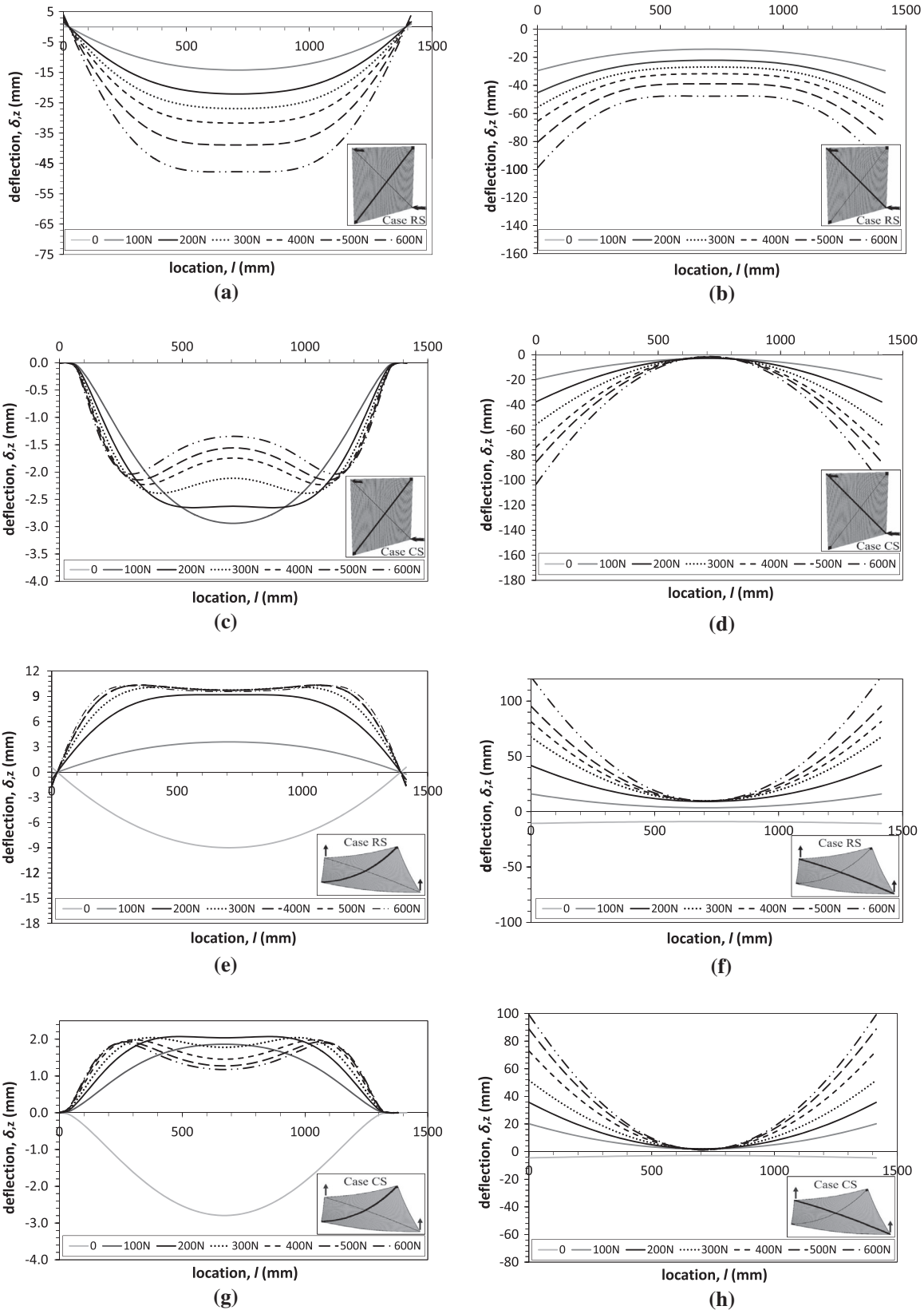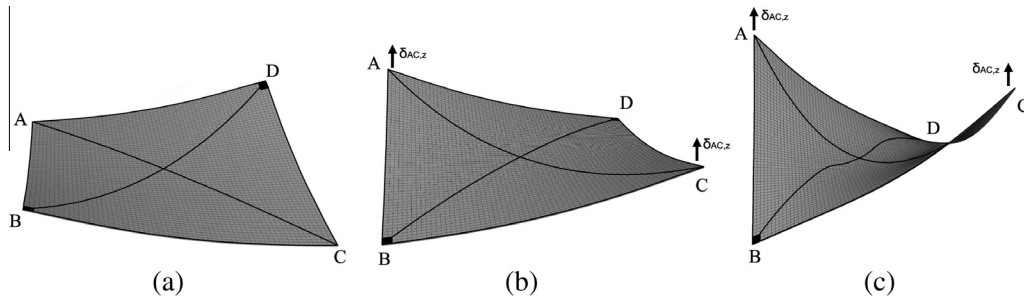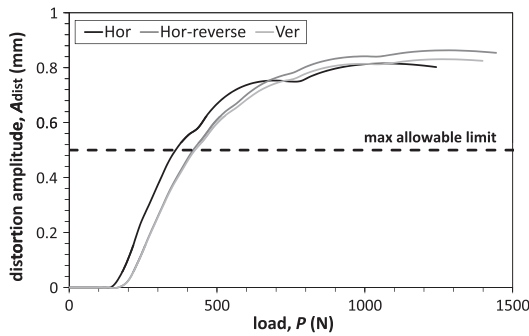
Fig. 15. Influence of the orientation of the plate on the profiles of the support and the load axes. (a) and (b) *Ver* testing for Case RS; (c) and (d) *Ver* testing for case CS; (e) and (f) *Hor*-reverse testing for Case RS; (g) and (h) *Hor*-reverse testing for Case CS (numerical data).

Fig. 16. Deformed plate shape for Case RS in *Hor*-reverse testing: (a) under self weight prior to the cold bending; (b) after snap-through instability occurred at a corner displacement of 15 mm; (c) after the cold bending distortion occurred at a corner displacement of 63 mm (exaggerated 30 times vertically).

Table 4
Snap-through instability and cold bending distortion for different plate orientations for Case CS and RS (✔ for occurrence, ✗ for absence).

	Case CS			Case RS		
	Hor	Hor-reverse	Ver	Hor	Hor-reverse	Ver
Snap-through buckling	✗	✔	✗	✗	✔	✗
Cold bending distortion	✔	✔	✔	✗	✔	✗

Fig. 17. Cold bending distortion amplitude for different plate orientations of Case CS.
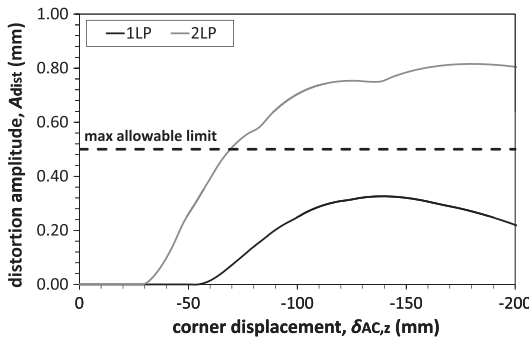
Fig. 18. Influence of the number of load points on the amplitude of the cold bending distortion.

reduced and is, in this instance, below the recommended limit for roller wave distortion (Fig. 18).

5. Conclusions

The aim of this study was to investigate and characterise the mechanical response of monolithic glass plates when subjected to cold bending into an anticlastic shape. Numerical modelling validated by experimental testing revealed that two phenomena

of interest, a change in the deformation mode and the cold bending distortion, may occur during the cold bending process.

The change in the deformation mode appears as the curvature of one diagonal continues to increase while, depending on the choice of boundary conditions, the curvature of the other diagonal decreases or remains constant. When in-plane displacement is restrained at the supported corners (Case CS & PS), the support axis becomes progressively stiffer during the change in the deformation mode, due to the membrane action mobilised by the boundary conditions at the supported corners. Therefore, significant deflections are confined to the load axis. This phenomenon occurs at an even earlier stage during the cold bending process if rotation is also restrained at the supported corners. However, when in-plane displacement is unconstrained (Case RS), the stiffness of the load axis increases and does not show a significant increase in curvature compared to the support axis.

Global instabilities (snap-through buckling) were only observed when the out-of-plane loads on the two free corners were applied in a direction opposite to the initial out-of-plane deflection induced by self-weight (or other surface imperfections) of the plate. This phenomenon appeared in the early stages of the cold bending process as an abrupt change of the direction of curvature in both diagonals and can be considered as a particular case of this change in the deformation mode.

The second phenomenon of interest during the cold bending process is the occurrence of a local instability (buckling). As the applied displacement at the loaded corners increases beyond the change in the deformation mode in Case CS and PS, a sinusoidal ripple, termed cold bending distortion, appears along the length of the support axis. This phenomenon followed in all the cases where snap-through instability had occurred i.e. even when in-plane displacement was allowed at the supported corners (Case RS). Therefore, the cold bending distortion is a function of boundary conditions and preceding global instabilities that are influenced by the combination of the self-weight and the direction of the applied load. This ripple can have a detrimental effect on the aesthetic quality of the curved plate as it may cause unwanted optical distortions, thereby triggering a serviceability limit state failure of cold bent glass.

The amplitude of the cold bending distortion can be used to evaluate the optical quality of the curved glass plate as recommended in EN 12150-1:2000 [3]. The parametric analysis performed in this study, revealed that the amplitude of the cold bending distortion is very sensitive to the choice of boundary conditions, geometrical characteristics of the plate and load locations. Larger distortion amplitudes were found in plates with pin supports (Case PS), larger thickness or larger aspect ratio.

All of the above parameters should be taken into account during the design of cold bent glass plates in order to avoid snap-though instabilities and to ensure the optical quality of the curved plate. An optical quality evaluation procedure is proposed in Appendix A for the cold bending of glass plates in a horizontal position, with two clamped corner supports (Case CS) and loaded at the

remaining two free corners in the direction of the self-weight to avoid snap-through instabilities. This evaluation procedure can be used to determine the applied displacement at which cold bending distortion occurs and to quantify its amplitude, thereby providing a measure of the optical quality of the cold bent glass plate.

Further research could include the use of thin plate theory as a third means of validating the experimental and numerical results performed in this study. Finally, safety reasons, often dictate that monolithic glass should not be used for structural applications. Therefore, future investigations should also include cold bent laminated glass, where the polymer interlayer between the two glass plates is expected to influence the mechanical response during cold bending as a function of temperature and strain-rate.

Acknowledgements

Appendix A. Procedure for evaluating the optical quality of cold bent monolithic glass plates

An optical quality evaluation procedure for predicting cold bending distortion in cold bent monolithic glass plates in anticlastic shapes is proposed in this section. This evaluation procedure is not a comprehensive design guide for cold bent glass, because among other things, the strength of glass is not considered. The evaluation procedure therefore provides the serviceability limit checks required to achieve an acceptable optical quality of the curved monolithic plate at the end of the cold bending process. For brevity, results are only provided for glass plates that are supported at two corners with the boundary conditions of Case CS. The evaluation procedure is based on a numerical parametric analysis that was performed for plates of different geometrical characteristics. In particular, plates with different thickness, aspect ratio (rectangular plates) or length ratio (square plates of different sizes) were considered in order to populate three dimensional charts, from which two dimensional views are taken and shown in Figs. A2 and A3. The charts are useful for establishing the applied corner displacement at which the cold bending distortion occurs and for determining the amplitude of the cold bending distortion. This evaluation procedure is valid for: (a) square plates with edge length, L, and thickness, h, ranging between 1000 mm to 3000 mm and 2 mm to 8 mm, respectively and; (b) rectangular plates with edge length, L, ranging between 500 mm and 2000 mm while the other edge length is 1000 mm. Their thickness also ranges between 2 mm and 8 mm.

The proposed procedure for assessing cold bending distortion is as follows (Fig. A1):

(1) Define the geometrical characteristics of the glass plate. These include the thickness of the plate, h, the length ratio,
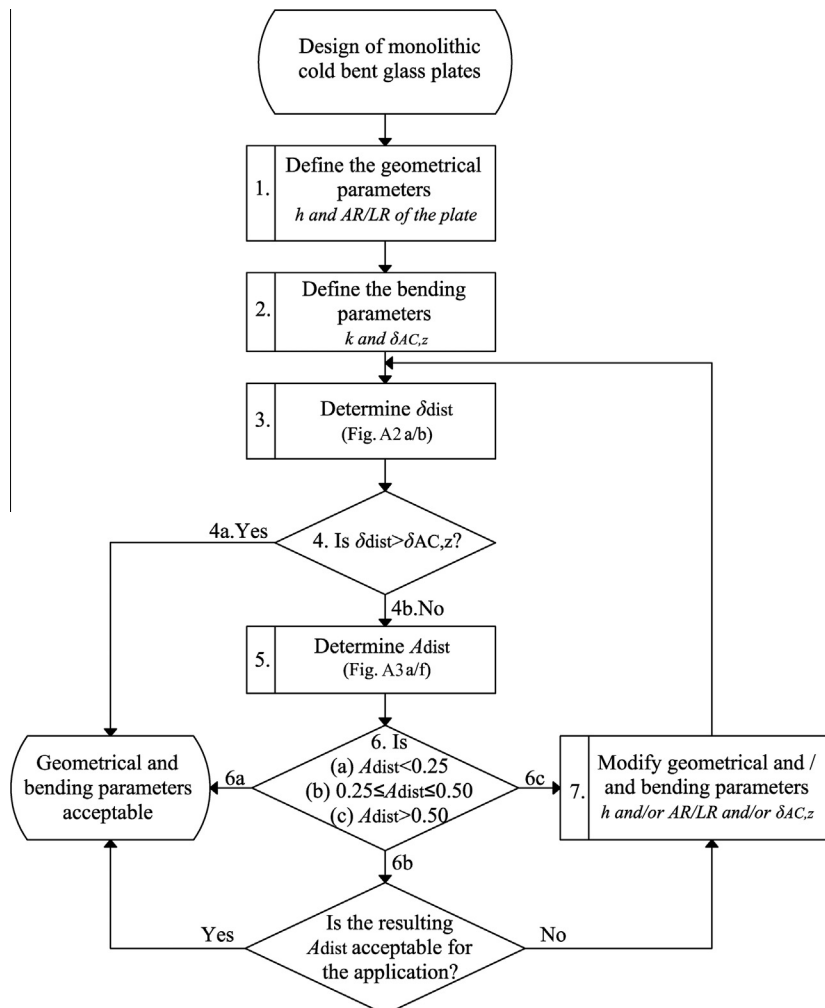

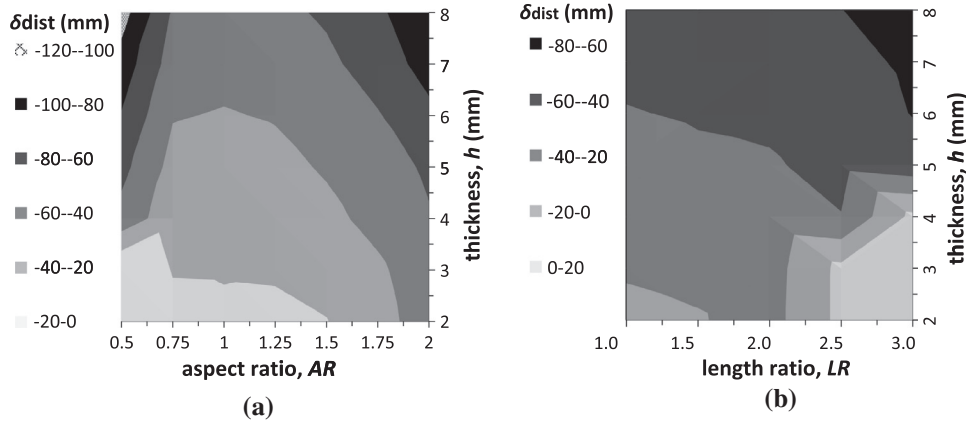**Fig. A1.** Optical quality evaluation procedure for cold bent monolithic glass plates.

Fig. A2. Applied displacement at the onset of the cold bending distortion for plates of different thickness and: (a) aspect ratio AR and; (b) length ratio LR (numerical data).
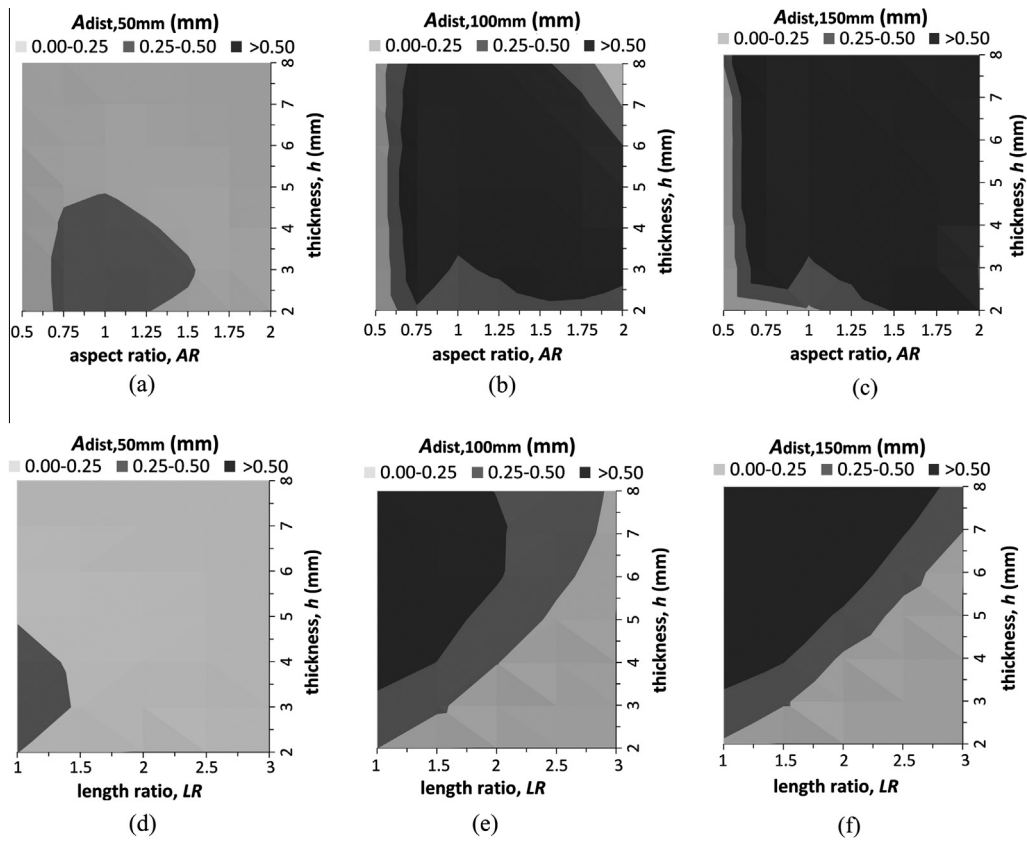

Fig. A3. Cold bending distortion amplitude for plates of different thickness and: (a)–(c) aspect ratio AR and; (d)–(f) length ratio for: (a and d) 50 mm; (b and e) 100 mm and; (c and f) 150 mm of applied displacement (numerical data).

LR for square plates or the aspect ratio, *AR*, for rectangular plates.

(2) Define the desired cold bending characteristics i.e. the curvature, κ, and consequently the forced displacement, $\delta_{AC,z}$, that is to be applied at the two free corners of the plate to produce the desired curvature. These would typically be determined from a finite element analysis of the plate on a case-by-case basis or from simple geometrical calculations based on the desired radius of curvature;

(3) Determine the applied displacement that triggers the onset of the cold bending distortion, δ_{dist} (Fig. A2).

(4) Establish whether cold bending distortion occurs in the process of achieving the desired cold bending geometry i.e. if $\delta_{dist} < \delta_{AC,z}$ (Fig. A2a/b).

(4a) If $\delta_{dist} > \delta_{AC,z}$ the desired geometrical and cold bending characteristics do not cause cold bending distortion and the optical quality is therefore unaffected.

(4b) If $\delta_{dist} < \delta_{AC,z}$, cold bending distortion occurs and the distortion amplitude, A_{dist}, should be quantified in order to determine whether it exceeds an acceptable value of distortion (e.g. limits set in EN12150-1:2000).

(5) Use the desired forced displacement at the free corners, $\delta_{AC,z}$, in Fig. A3a–f to quantify the distortion amplitude.

(6) Determine whether the distortion amplitude exceeds 0.25 mm or another user-prescribed value.

(6a) If $A_{dist} < 0.25$ mm then the amplitude is considered acceptably low and its effect on the optical quality is negligible.

(6b) If $0.50 \geqslant A_{dist} \geqslant 0.25$ mm, the cold bending distortion could be visible depending on the location and the incidence of reflections on the glass.

(6c) If $A_{dist} > 0.50$ mm, the cold bending distortion will be clearly visible and is deemed unacceptable.

(7) If A_{dist} calculated from step 6, is considered unacceptable, the geometrical and/or bending parameters should be modified accordingly and the cold bending distortion is re-assessed from step (3).

Appendix B. Supplementary material

Supplementary data associated with this article can be found, in the online version, at http://dx.doi.org/10.1016/j.engstruct.2016.03.019.

References

[1] NSG Group. Pilkington and the Flat Glass Industry 2010. <www.pilkington.com/pilkington-information/downloads/pilkington+and+the+flat+glass+industry+2010.htm> [last accessed June 2015].

[2] Eekhout M. Design, engineering, production & realisation of glass structures for "free-form" architecture. CWCT members meeting. Bath, United Kingdom; 2004.

[3] CEN (European Committee for Standardization). Glass in building. Thermally toughened soda lime silicate safety glass – Part 1: Definition and description. EN 12150-1:2000; 2000.

[4] ASTM Standard C1651-11. Measurement of roll wave optical distortion in heat-treated flat glass1. West Conshohocken (PA): ASTM International; 2011. http://dx.doi.org/10.1520/C1651-11. <http://www.astm.org>.

[5] Abbott A. Roller wave distortion. Definition, causes and a novel approach to accurate on-line measurement. In: Proc glass processing days, Finland; 2001. p. 226–30.

[6] Marradi B. Function follows form. Strategies for integrated design of complex glass envelopes. In: Proc challenging glass 3 & COST action TU0905 mid-term conf, Croatia; 2013. p. 61–8.

[7] Neugebauer J. Applications for curved glass in buildings. J Façade Design Eng (JDFE) 2014;2:67–83.

[8] Teich M, Kloker S, Baumann H. Curved glass: bending and applications. In: Proc engineered transparency conf, Germany; 2014. p. 75–83.

[9] Weber F. Curved glass structures. In: Proc glass performance days, Finland; 2009. p. 375–80.

[10] Von Starck A, Muhlbauer A, Kramer C. Handbook of thermoprocessing technologies, fundamentals, processes, components, safety. Vulkan-Verlag GMbH; 2005. p. 605–12.

[11] Saksala M. Curved and tempered glass – demand, challenge and opportunity for the market driven technology. In: Proc glass performance days, Finland; 2003. p. 63–5.

[12] Galuppi L, Royer-Carfagni G. Rheology of cold-lamination-bending for curved glazing. Eng Struct 2014;61:140–52.

[13] Galuppi L, Royer-Carfagni G. Cold-lamination-bending of glass: sinusoidal is better than circular. Compos B – Eng 2015;79:285–300.

[14] Overend M. Recent development in design methods for glass structures. Struct Eng 2010;88(14):18–26.

[15] Overend M, Zammit K. A computer algorithm for determining the tensile strength of float glass. Eng Struct 2012;45:68–77.

[16] Haldimann M, Luible A, Overend M. Structural use of glass. International Association for Bridge and Structural Engineering (IABSE); 2008.

[17] Zaccaria M, Overend M. Thermal healing of realistic flaws. J Mater Civ Eng 2016;28(2):04015127.

[18] Chinzi G. Curved glass surfaces: design, process definition & performances. In: Proc glass performance days, Finland; 2013. p. 336–44.

[19] Fildhuth T, Knippers J. Double curved glass shells from cold bent glass laminates. In: Proc glass performance days, Finland; 2011. p. 384–9.

[20] Dodd G, Thieme S. Comparison of curved glass and cold bent panels. In: Proc glass performance days, Finland; 2007. p. 83–6.

[21] Saksala M. Extraordinary shapes with ordinary costs. In: Proc glass performance days, Finland; 2005. p. 371–3.

[22] Feijen M, Vrouwe I, Thun P. Cold-bent single curved glass; opportunities and challenges in freeform facades. In: Proc challenging glass 3 & COST action TU0905, Delft; 2012. p. 829–36.

[23] Vollers K, Veer F. Usage of cold bent glass panes as an approximation for double curved surfaces. In: Proc glass processing days, Finland; 2003. p. 173–5.

[24] Manara G, Florian C, Tonon L. Cold twisting in point fixed glass: a case study. In: Proc XXV A.T.I.V. int conf, Parma; 2010.

[25] Eekhout M, Lockefeer W, Staaks D. Application of cold twisted temped glass panels in double curved architectural design. In: Proc glass performance days, Finland; 2007. p. 213–20.

[26] Eekhout M, Niderehe S. The new, cold bent glass roof of the Victoria & Albert Museum, London. In: Proc glass performance days, Finland; 2009. p. 408–12.

[27] Vakar L, Gaal M. Cold bendable laminated glass – new possibilities in design. Struct Eng Int 2004;14:95–7.

[28] van Herwijen E, Staaks D, Eekhout M. Cold bent glass sheets in façade structures. Struct Eng Int 2004;14(2):98–101.

[29] Eekhout M, Staaks D. Cold deformation of glass. In: Proc int symp application of architectural glass ISAAG, Germany; 2004.

[30] Galuppi L, Massimiani S, Royer-Carfagni G. Large deformations and snap-through instability of cold bent glass. In: Proc challenging glass 4 & COST action TU0905 final conf, Switzerland; 2014. p. 681–90.

[31] Galuppi L, Massimiani S, Carfagni GR. Buckling phenomena in double curved cold-bent glass. Int J Non-Linear Mech 2014;64:70–84.

[32] Datsiou K, Overend M. Behaviour of cold bent glass plates during the shaping process. In: Proc engineered transparency int conf, Dusseldorf; 2014. p. 125–34.

[33] Beer B. Complex geometry facades – introducing a new design concept for cold-bent glass. In: Proc glass performance days, Finland; 2013. p. 516–22.

[34] Belis J, Inghelbrecht B, van Impe R, Callewaert D. Cold bending of laminated glass panels. HERON 2007;52(1/2):123–6.

[35] Belis J, Inghelbrecht B, van Impe R, Callewaert D. Experimental assessment of cold-bent glass panels. In: Proc glass performance days, Finland; 2007. p. 115–7.

[36] Scattered Light Polariscope SCALP Instruction Manual, Ver. 5.5, GlasStress Ltd.

[37] Abaqus 6.12 Documentation. Analysis User's Manual, Simulia; 2012.